Materials Research. 2019; 22(6): e20190462
DOI: http://dx.doi.org/10.1590/1980-5373-MR-2019-0462

Deformation and Solidification Characteristics and Microstructure of Arc Sprayed Ni-Al Composition Coatings

Jixiao Wang[a,b], Jun Wang[a], Guo Jin[a], Li Wang[b]*, Caisong Mo[b], Li Ma[b], Hongxian Shen[c], Fuyang Cao[c], Jianfei Sun[c]

[a] *National University Science Park, Harbin Engineering University, 150001, Harbin, China*
[b] *School of Mechanical and Electrical Engineering, Guangdong University of Petrochemical Technology, 525000, Maoming, China*
[c] *School of Materials Science and Engineering, Harbin Institute of Technology, 150001, Harbin, China*

Received: August 11, 2019; Revised: November 24, 2019; Accepted: December 11, 2019

Droplets deformation and solidification characteristics in twin-wire arc sprayed Ni-Al were explored in depth. Both theoretical method and numerical model were established for calculating the deformation process of the droplets impacting on the substrate and their solidification behavior in airflow, which based on two models of the volume of fluid (VOF) dual-phase flow and the standard k-ε. The morphology and the microstructure of the composite coatings were analyzed by XRD, SEM and TEM. The results of the experiment indicate the droplets cooling rate ranges from 3.0×10^7 to 7.5×10^7 K/s. The main components of Ni-5wt.% Al coating were Ni solid solution, and a small number of Ni_3Al_4, Al_2O_3 and NiO. The main phases of Ni-20wt.% Al coating are Ni_3Al and NiAl. EDS and TEM analysis shows that there are a few amorphous and equiaxed crystals in the Ni-Al coating. The surface roughness increases with the decrease of spraying pressure and spraying distance.

Keywords: *arc spraying, droplet, deformation and solidification, composition coating.*

1. Introduction

In the process of twin-wire arc spraying (TWAS), the droplets generated by arc are atomized into smaller droplets within a certain size range by dry compressed airflow. The deformation size and solidification characteristic of the droplets greatly affect the microstructure and properties of the coating. Thus, analyzing the deformation and solidification characteristic of the droplets can improve the properties of coatings, build the internal relationship between them, which can also evaluate the quality of coatings and provide effectively technical basis through optimizing arc spraying process parameters.

Many scholars have studied in detail on the breakup of the droplets under certain flow field conditions. Blackwell BC[1] and Weng KW[2] had explored the behavior of the droplets flight in low velocity region in natural airflow. Kelkar M[3] investigated that the atomized droplets are divided into primary and secondary crushing. They simulated the deformation and breakup process of the droplets, and analyzed the breakup form and influence factors. Wang JX[4] calculated the dynamic characteristics of spraying droplets and the atomization behavior. The atomization law of TWAS droplets is verified by the particles velocity characteristics, and which provides a reference for obtaining the best spraying process parameters. However, the impact deformation and solidification behavior between the droplets and the substrate after fragmentation have not been studied, especially about arc spraying. For calculating the droplets deformation and solidification process, the VOF and the standard k-ε models are combined to build a numerical method. The deformation and solidification process of two kinds of size droplets at different velocities are analyzed in this paper.

TWAS is a process of arc generation by positive and negative wires. High temperature droplets are produced by melted wires, and then the droplets are atomized by compressed air to produce high velocity dual-phase flow, which sprays onto the substrate and forms a certain density coating. To simplify the problem, interrelations of the droplets are neglected. The transport characteristic of the droplets is described in the spray gas flow. It is assumed that the droplets by the TWAS high-velocity gas flow producing are the isothermal fluid and the droplets are supposed to be spherical. The deformation of the droplets impacting on the substrate with the droplets size and velocity and their solidification behavior are systematically analyzed.

2. Deformation and Solidification Behavior of Atomized Droplets

The deformation and solidification behavior of the droplets impacting on the substrate after TWAS atomization have very important effects on the bonding strength, porosity and surface roughness of the coating. In some thermal barrier coatings, it is desirable to obtain higher porosity[5, 6]. The larger the average diameter of molten particles is, the smaller the porosity of the coating is. With the decreasing of the atomized droplets size, the surface roughness of the coating decreases[7].

The flat deformation occurs when the droplets impact on the substrate. The higher the impact velocity, the greater the pressure acting on the surface of the substrate, so the coating density is the greater, and the bonding force of the flat

*e-mail: wangliwangli_1@163.com

particles is the greater. Therefore, it is of great significance to study the deformation and solidification characteristics of Ni-Al droplets when high-velocity impacting on the substrate. The VOF model is used to follow the tracks of the free surface and solidification interface of the droplets-substrate deformation. A theoretical model of the droplets-substrate deformation and solidification is built. The impact deformation and solidification process of the droplets with different diameters under different velocities are analyzed.

2.1 Numerical modeling and material physical parameters

In the governing equation VOF dual-phase flow model is adopted. The governing equation includes continuity equation, energy equation and momentum equation. Assuming that the volume is incompressible and the density of the droplets is constant. The two-dimensional continuity equation is as follows:

$$\frac{\partial u}{\partial x}+\frac{\partial v}{\partial y}=0 \qquad (1)$$

In the formula u and v are the velocities of droplets in the x and y directions respectively. Momentum equation is used to solve the problem. The momentum equation group and the obtained velocity field are all gas-liquid dual-phase shared.

$$\rho\frac{du}{dt}=\mu\left(\frac{\partial^2 u}{\partial x^2}+\frac{\partial^2 u}{\partial y^2}\right)-\frac{\partial \rho}{\partial x}+G_x \qquad (2)$$

$$\rho\frac{dv}{dt}=\mu\left(\frac{\partial^2 v}{\partial x^2}+\frac{\partial^2 v}{\partial y^2}\right)-\frac{\partial \rho}{\partial y}+G_y \qquad (3)$$

In the formula, p is pressure, μ is dynamic viscosity, and G_x and G_y are transverse and longitudinal volumetric forces, respectively. Density $\rho = (1 - F)\rho_1 + F\rho_2$, F is the volume fraction of the target fluid in each unit. ρ_1 is the air density, and ρ_2 is the droplet density.

The energy of molten droplets includes thermal energy and mechanical energy. The heat transformed by mechanical energy is very little compared with the heat carried by the molten droplets themselves, so this part of the heat can be neglected. Therefore, the energy conservation equation can be simplified as follows:

$$\rho c_V\frac{dT}{dt}=\lambda\left(\frac{\partial^2 T}{\partial x^2}+\frac{\partial^2 T}{\partial y^2}\right) \qquad (4)$$

In the formula, T is the temperature, c_V is the specific heat capacity, and λ is the thermal conductivity. In the VOF model, the temperature T in each unit is taken as the average of the mass fraction of each phase. T_1 and T_2 of each phase in the formula are calculated based on the thermo physical parameters of the phase.

$$T=\frac{(1-F)\rho_1 T_1+F\rho_2 T_2}{(1-F)\rho_1+F\rho_2} \qquad (5)$$

The molten droplet is defined as the target fluid, and the volume fraction F of each unit is the ratio of the volume of the target fluid to the total volume of the unit. Assuming that the two target fluids in the computational region occupy the regions of Ψ and Ψ', and the free surface is Γ, (i, j) as the unit coordinate. There are $F = 1$, (i, j) ∈Ψ; $0 < F < 1$, (i, j) ∈Γ; $F = 0$, (i, j) ∈Ψ›. Then the VOF governing equation is as follows:

$$\frac{\partial F}{\partial t}+u\frac{\partial F}{\partial x}+v\frac{\partial F}{\partial y}=0 \qquad (6)$$

The F values of all elements can be obtained by solving the above formula, and the updated free surface Γ can be obtained by connecting the grids whose F values are between 0 and 1.

The droplet exchanges heat with the surrounding medium, and solidification occurs when the temperature of the droplet drops below the melting point temperature. The solidification begins at the base of the droplet, and the solidification interface moves continuously with the loss of heat until the whole droplet becomes solid. In order to distinguish the solid phase and the liquid phase in a droplet, the volume fraction γ of unit liquid phase is defined. By calculating the unit γ value, the solidification interface can be traced. In order to make all elements of the whole calculation area meaningful to γ, the γ values of gas region unit and solid region (substrate) unit are defined as 1 and 0 respectively. The internal unit γ value of the droplet is defined as: γ=0，$T \le T_m$；γ=1，$T > T_m$（T_m is metal melting point）.

The calculated area size and partitioned grids are as follows. The fluid region is 500 μm×55 μm, and 28×250 grids. The solid region is 500 μm×55 μm and 20×250 grids, a total of 12000 grids. The computational region diagram and boundary conditions are shown in Figure 1. According to the size characteristics of Ni-Al powders obtained during twin-wire arc spraying[8], droplets with diameter of 25 μm and 50 μm were selected to analyze the impact deformation and solidification behavior of single droplet. The negative velocity of the droplet impacting on the substrate along the y axis is 100 m/s, 200 m/s, 300 m/s and 400 m/s, respectively. The physical parameters of the materials used for calculation are shown in Table 1.

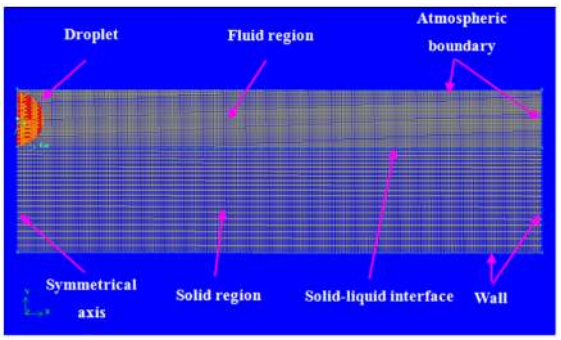

Figure 1. Diagram of calculation region.

Table 1. Thermo physical parameters for numerical analysis.

Materials	ρ	T	λ×10²	μ×10⁶	C_v	M	σ
	(kg/m³)	(K)	W/(m·K)	kg/(m·s)	kJ/(kg·K)	(g/mol)	(N/m)
Ni-5wt%Al	8591	1728	9727.3	5000	481.12	57.1	1.778
Air	1.225	-	2.42	17.89	1.006	28.97	-
6061-T6	2.71	925.2	20240	-	871	-	-

2.2 Analysis of droplet impact deformation and solidification

As can be seen from Figure 2 to Figure 4, when the droplets impact on the substrate, they spread out and form flattened particles. As time goes on, the flatness of the droplets becomes more serious (the temperature of each point in the droplets is above the liquidus temperature, and there is no solidification layer at 0 s). In the process of the droplet spreading on the substrate, heat exchange will take place with the surrounding medium, and the solidification layer will be formed and grow up. The solidification interface inside the droplet will gradually enlarge, when it spreads around and moves upward continuously. The solidification interface leans slightly from the middle to the surroundings, and tends to be horizontal gradually with the increase of time. The lower the impact velocity of the droplet is, the slower the droplet spreading is in the same time range of 1 μs. To the same droplet impact velocity, the smaller droplet size is, the smaller flat particle thickness is. In the case of high-velocity impact, the smaller-size droplets will form the smaller-diameter flat particles. At the far center of the axis, the high-velocity droplets will seriously spatter when impacting on the substrate.

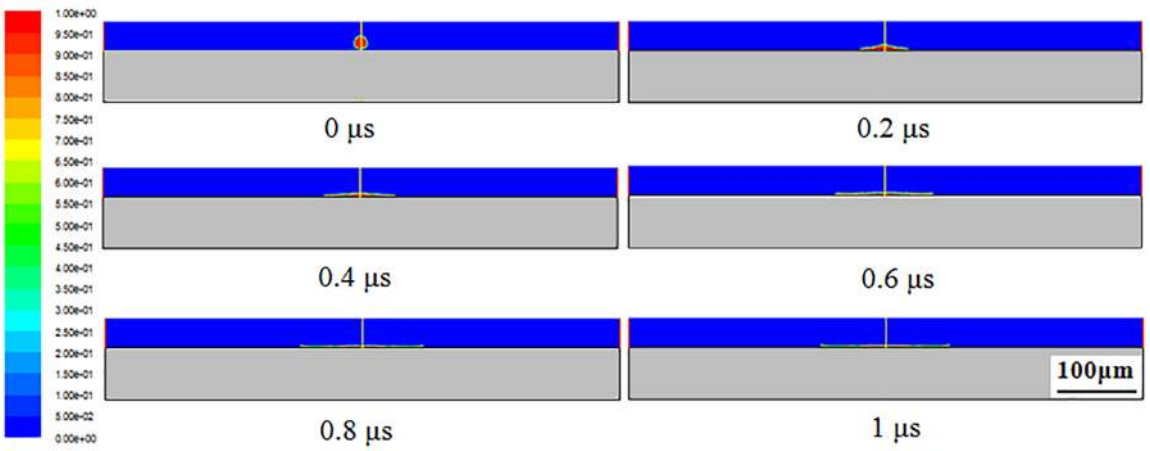

Figure 2. Deformation and solidification process of TWAS droplet (ø25 μm, 100 m/s).

Figure 3. Deformation and solidification process of TWAS droplet (ø50 μm, 100 m/s).

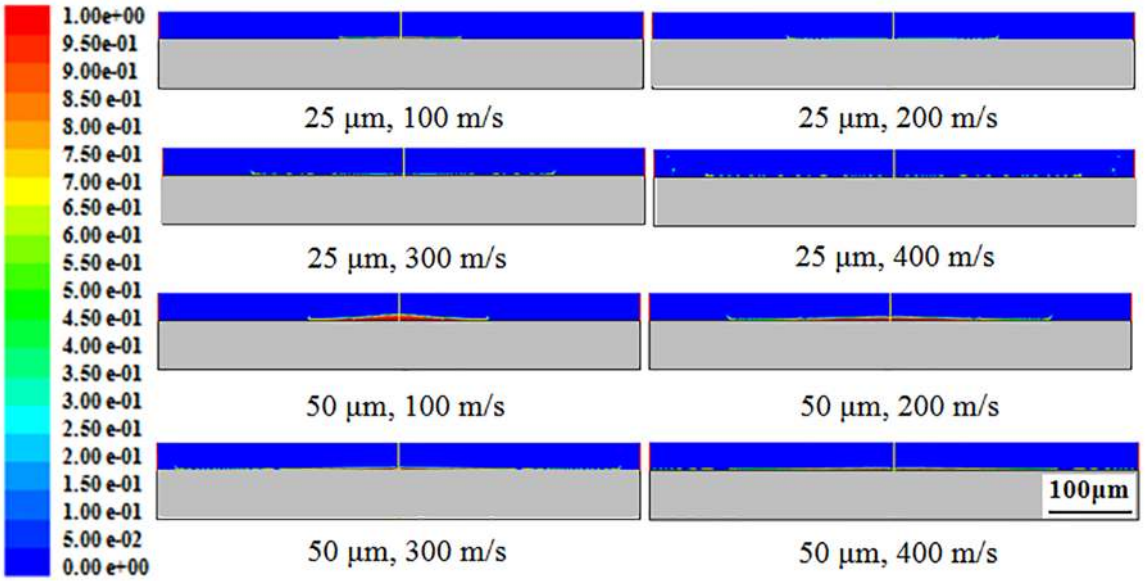

Figure 4. Changes of droplet deformation and solidification with diameter and velocity at 1 μs.

Figure 5 shows the relationships between the diameter and the thickness of droplet spreading and solidification time. With the decrease of the deformation time, the spread diameter shows a decreasing trend. Meanwhile, the smaller droplet diameter and the lower velocity are corresponding to the smaller spreading diameter. The spreading diameter tends to be stable after 1 μs. As shown in Figure 5b, the spreading thickness is decreased with the increase of deformation time. The spreading thickness is enhanced with the decrease of the velocity and the increase of the droplet volume.

2.3 Analysis of temperature field of droplets

Figure 6 to Figure 8 show droplet diameters of 25 μm and 50 μm, and the solidification temperature fields at different velocities (100 m/s, 200 m/s, 300 m/s and 400 m/s) vary with time, and the unit of temperature field is K.

From Figure 6 to Figure 8, it can be seen that the radius of flat particles increases with the prolongation of the spreading time of the droplets on the substrate. The temperature field is centered on the y axis and expands around it. Because of the high velocity at the center of the axis, the temperature decreases rapidly. The solidification of the droplet with a diameter of 25 μm is faster than that of the droplet with a diameter of 50 μm in the range of 1 μs. With the decrease of impact velocity, the temperature field of the droplet with the same diameter reduces, and a small temperature gradient changes far from the center of the axis, which will affect the solidification of surrounding particles.

Figure 9 is the relationship between solidification temperature and time of droplets in twin-wire arc spraying. The maximum temperature is extracted at different time and the solidification temperature is calculated to 50 μs

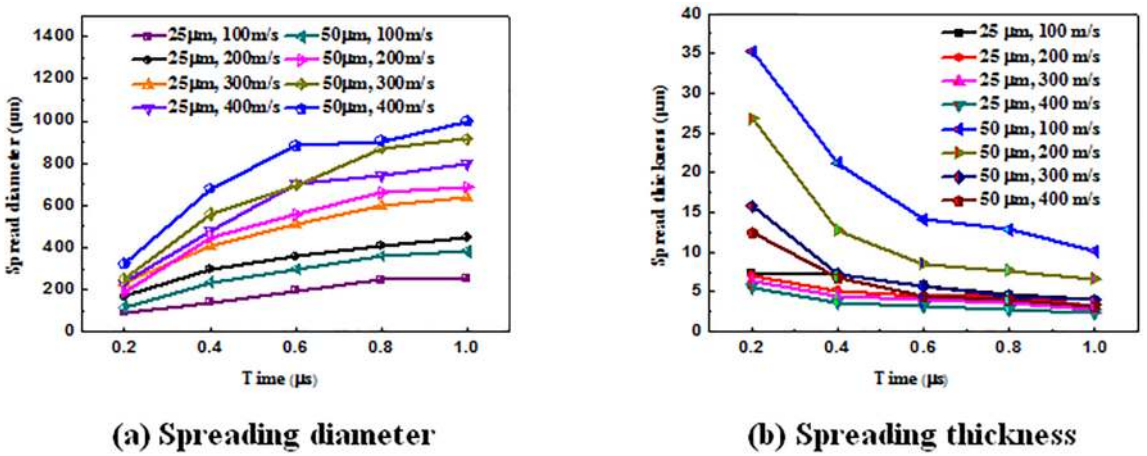

Figure 5. Relationships between droplet spreading diameter and thickness and solidification time for (a) and (b).

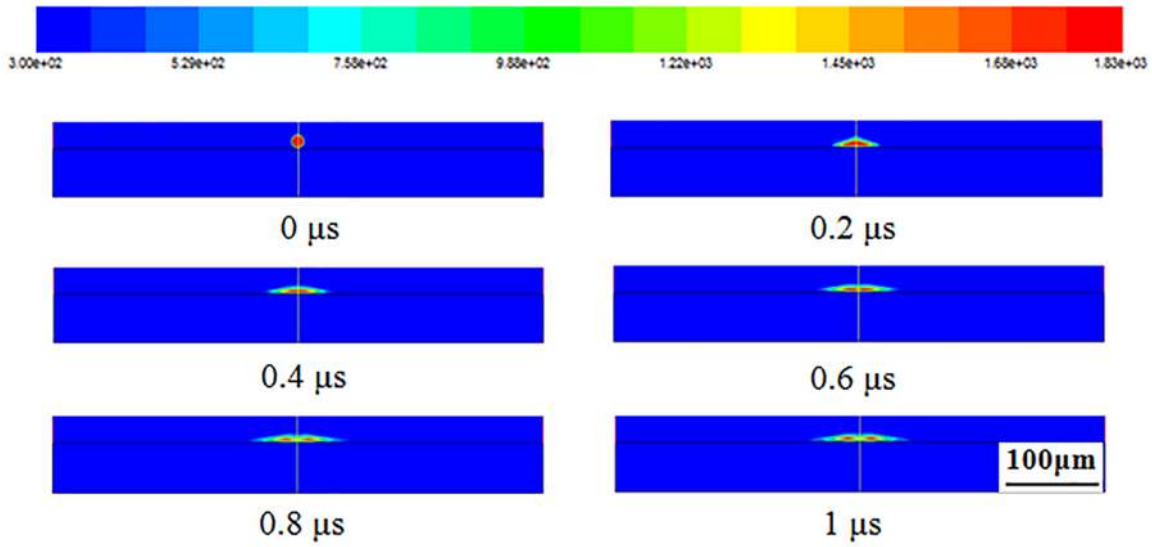

Figure 6. Change of solidification temperature field of TWAS droplet (ø25 μm, 100 m/s).

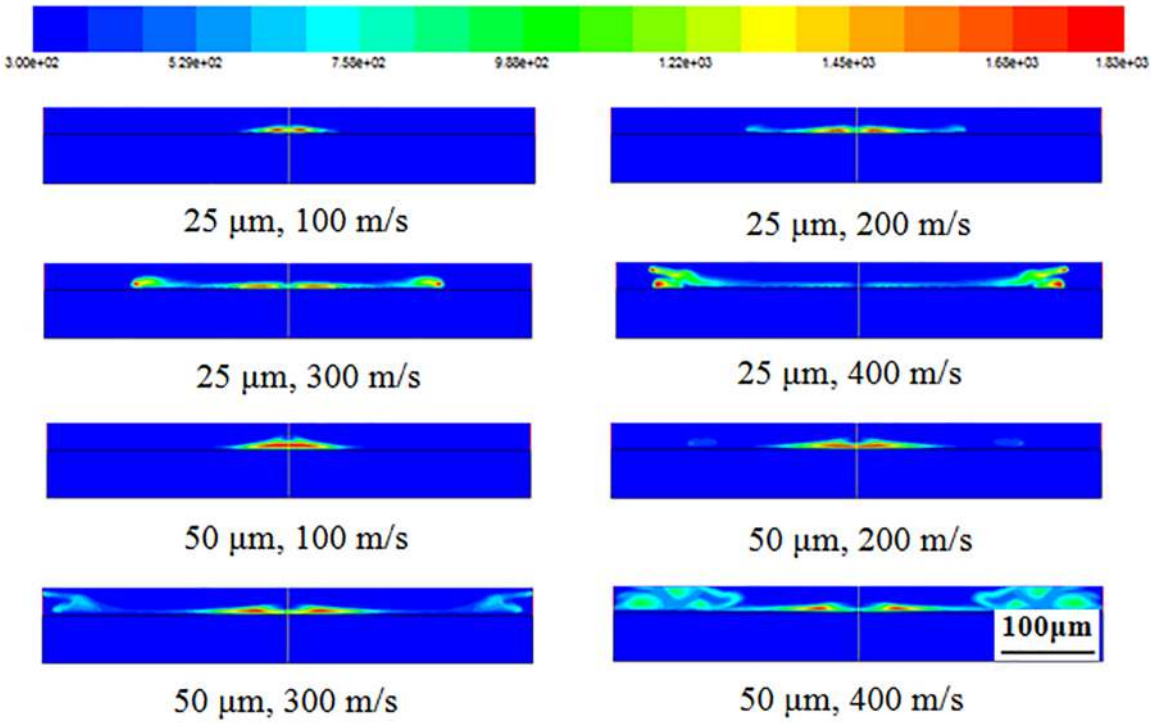

Figure 7. Change of solidification temperature field of TWAS droplet (ø50μm, 100 m/s).

under each parameter. From Figure 9, it can be seen that the cooling rate of the droplets of 50 μm and 25 μm is much faster in the range of 0 ~ 10 μs than that of between 10 μs and 50 μs. The cooling rate is the slowest in the range of 0 ~ 40 μs while the droplet diameter is 50 μm and the velocity is 100 m/s. The cooling rate is the fastest in the range of 0 ~ 40 μs while the droplet diameter is the velocity is 25 μm and the velocity is 400 m/s. By calculating the solidification rate of the droplets ranged from 3.0×10^7 to 7.5×10^7 K/s. Therefore, solidification characteristic of the droplets of twin-wire arc spraying is the rapid solidification.

The droplet will exchange heat with its surroundings accompanied by its deformation. Its solidification state and deformation degree interact with each other. Temperature reflects the parameters of energy distribution in the calculation area. The initial temperature of the Ni-Al droplets is 1828 K, and the initial temperature of substrate and air is 300 K. The heat of the droplets is transferred to the air and substrate. The

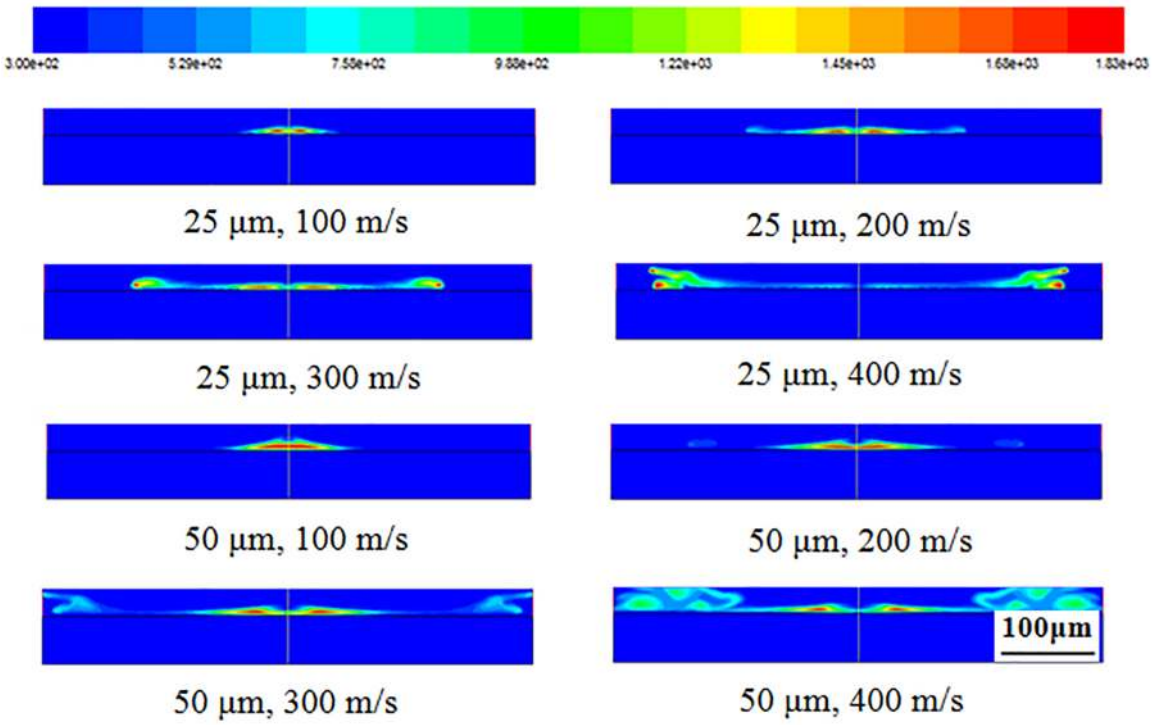

Figure 8. Change of solidification temperature field of TWAS droplet at 1 μs.

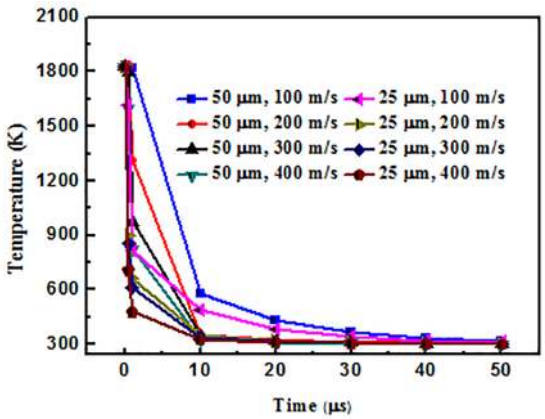

Figure 9. Relationships between droplet solidification temperature and impact times.

temperature of the droplets decreases gradually from the center to the surroundings. Due to the influence of the subsequent droplet particles on the former droplet particles, while the former droplet is in a state of semi-solid, the latter droplet gets to the surface of the former droplet in the actual spraying process. Little heat will be exchanged with the subsequent droplets but the heat of the droplet is mainly transferred to the substrate which contacts the droplet. At the same time, many pits are formed on the droplets surface because of the high velocity of the droplets, and the temperature field fluctuates far from the center of the axis.

3. Microstructure and Performance of Composition Coating

In arc spraying, arc is generated between two conductive wires, a tiny molten pool is generated at the tip of conductive wires, and the droplet in melting state is produced under the action of arc gravity field, gravity field and surface tension. Kelkar M[9] believed that under the action of atomized gas, primary and secondary dispersed droplet particles were formed successively. Hsian LP[10] observed that the size distribution of secondary dispersed droplet particles obeyed a simple normal distribution. In the process of arc spraying, the smaller the atomization pressure is, the smaller the dragging force of the primary dispersed droplet particles will be. The shorter the time of metal droplets staying at the wire tip, the more the primary dispersed droplet particles detached from the wire tip per unit time will be under the condition of a certain wire feeding velocity, which will lead to flying droplets size decrease[11-14]. The deformation and solidification process of the droplets impacting on the substrate are analyzed, which will help to design a reasonable spraying process and play a positive guiding role.

3.1 Microstructure analysis of Ni-Al coating

Ni-20wt.% Al composite wire as the surface layer and Ni-5wt.% Al alloy wire was used as the bond layer. The composite coatings were prepared by twin-wire arc spraying. The microstructure and properties of the composite coatings were further analyzed. The diagram of spraying process is shown in Figure 10, and the process parameters of sandblasting and spraying are shown in Tables 2 and 3, respectively.

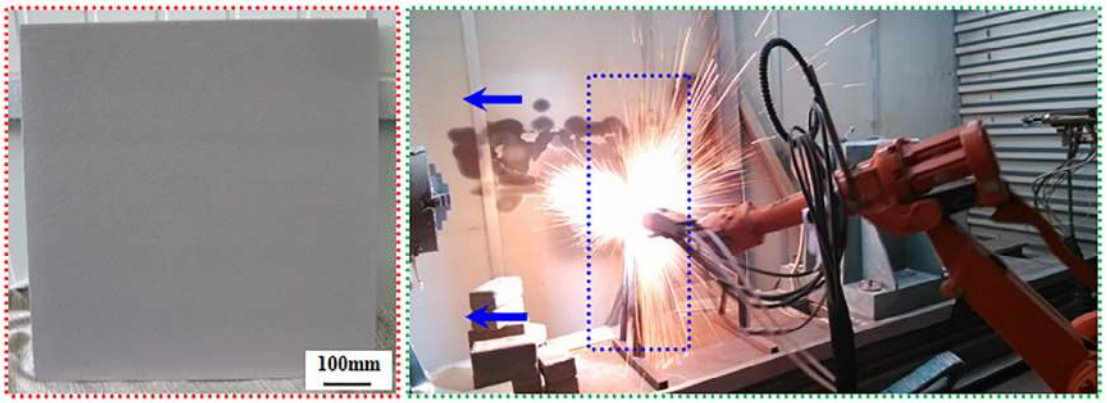

Figure 10. Process of the TWAS spraying Ni-Al composite coating for (a) and (b).

Table 2. Related sandblasting parameters before arc spraying.

Substrate	Carrier gas	Carrier gas pressure (MPa)	Distance (mm)	Sand material	Sand size (mm)	Time (s)	Angle (°)
6061-T6	Air	0.4~0.6	30~50	Al_2O_3	0.5	30	90

Table 3. Processing parameters of arc spraying.

Spraying materials	Spraying current (A)	Spraying voltage (V)	Air pressure (MPa)	Wire diameter (mm)	Gun velocity (mm·s^{-1})	Spraying distance (mm)	Coating thickness (mm)
Ni-5wt.%Al	260	38	0.5	ø1.6	300	150	0.15
Ni-20wt.%Al	240	36	0.5	ø1.6	300	50	0.35

X-ray diffraction analysis of Ni-Al coating prepared by D/MAX-2500 diffractometer was carried out. The microstructure of the coating was observed by Zeiss optical microscope and JEM 2010 transmission electron microscopy.

Figure 11a shows the X-ray diffraction results of Ni-5wt.% Al coating. From the diffraction pattern, it can be seen that the main constituent phase in Ni-5wt.% Al coating is Ni solid solution, including part of NiO, Al_2O_3 and Ni_3Al_4. This is because the content of Al is about 5% in Ni-Al alloy wire and its composition is a single Ni solid solution.

During twin-wire arc spraying, the end of wire is heated rapidly to melt under the action of arc heat source. At this time, part of aluminum in Ni solid solution will be precipitated from nickel solid solution and be exposed to air. Molten nickel and active aluminum will be oxidized with oxygen in air at high temperature, resulting in NiO and Al_2O_3. The following formulas should be used:

$$2Ni + O_2 \rightarrow 2NiO + Q \quad (7)$$

$$4Al + 3O_2 \rightarrow 2Al_2O_3 + Q \quad (8)$$

These reactions give off a lot of heat, which further increases the temperature of the droplets at the end of the wires. As a result, the heat loss of sprayed droplets is less while they get to the surface of the substrate, which makes it easy for the substrate to bond with the coating by micro-metallurgy. Therefore, the bonding strength between coating and substrate is improved[15-17].

The X-ray diffraction patterns of Ni-20wt.% Al coating in Figure 11b show that the main phases in the coating are Ni_3Al and NiAl. Because the nickel-aluminum composite wire is a powder core structure, the nickel powder and the aluminum powder are mixed in a certain proportion and put into the aluminum tube. The heating temperature of the end of the wire increases under the action of arc heat source when spraying. At a certain time, the nickel and aluminum in the nickel-aluminum composite wire react with each other. The reaction formula is as follows:

$$3Ni + Al \rightarrow Ni_3Al + Q \quad (9)$$

$$Ni + Al \rightarrow NiAl + Q \quad (10)$$

Ni_3Al and NiAl are formed in the coating on the substrate surface. This reaction releases a lot of heat, which is the main reason for the self-bonding performance of nickel-aluminum composite wire[18-20].

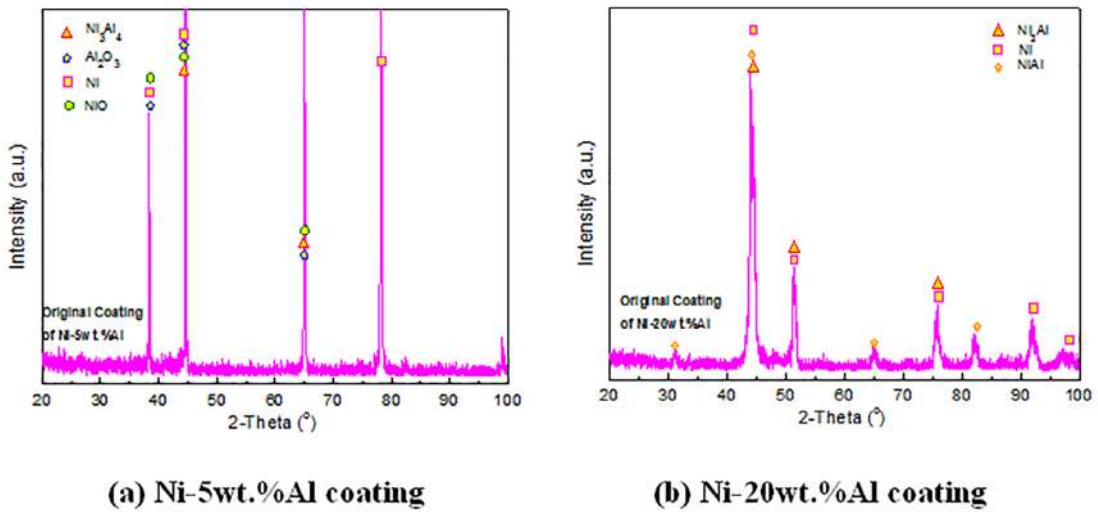

Figure 11. XRD patterns of as-prepared coating Ni-5wt.%Al and Ni-20wt.%Al for (a) and (b).

Figure 12 is a TEM analysis of the original state of Ni-Al coating. In the surface layer of the coating (Ni-20wt.% Al), the amorphous phase exists in the coating (Figure 12a) as shown by the selected area electron diffraction (Figure 12b) and EDS and elemental composition (Figure 12c). Figure 13 is TEM morphology and electron diffraction of the as-prepared Ni-Al coatings. From Figure 13a, it can be seen that there are equiaxed grains (2#) in the coating and the orientation of the [011] band axis of the selected area electron diffraction is Ni substrate. The existence of amorphous and equiaxed crystals is due to the formation of sprayed particles under rapid cooling conditions. Ni-Al particles exposed to the air react with oxygen to produce equivalent heat. At the same time, the Ni-Al particles are oxidized to varying degrees. The particles are impacted on the substrate in a melting or semi-melting state to form a coating. In this very short period of time, some phase structures in the coating can not change, and the original structure is directly retained in the coating. By XRD, EDS and TEM analysis, the coating is mainly composed of Ni solid solution, Ni-Al compound, Ni and Al oxides, mainly composed of Ni, Al and O elements.

3.2 Surface roughness of Ni-Al coatings

Surface roughness has a great influence on the properties of coatings. Surface roughness affects the wear resistance and corrosion resistance of coatings. Appropriate roughness is beneficial to improve the properties of coatings.

The relationships between spraying process parameters and surface roughness were studied. The surface state and three-dimensional morphology of the coating were observed by OLS 4100 laser confocal microscope, and the surface roughness of the coating was measured. Helios Nanolab 600i

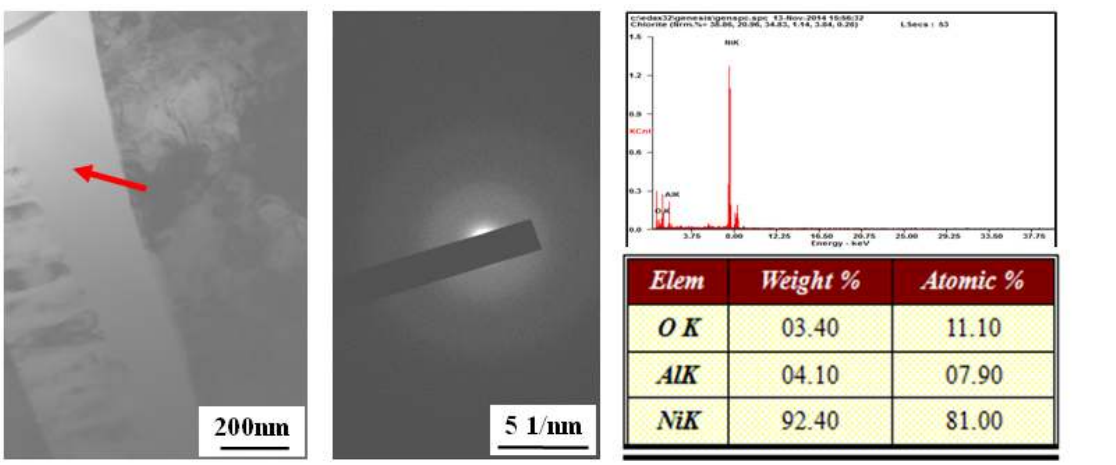

Figure 12. TEM morphology and electron microanalysis of the Ni-Al coatings for (a), (b) and (c).

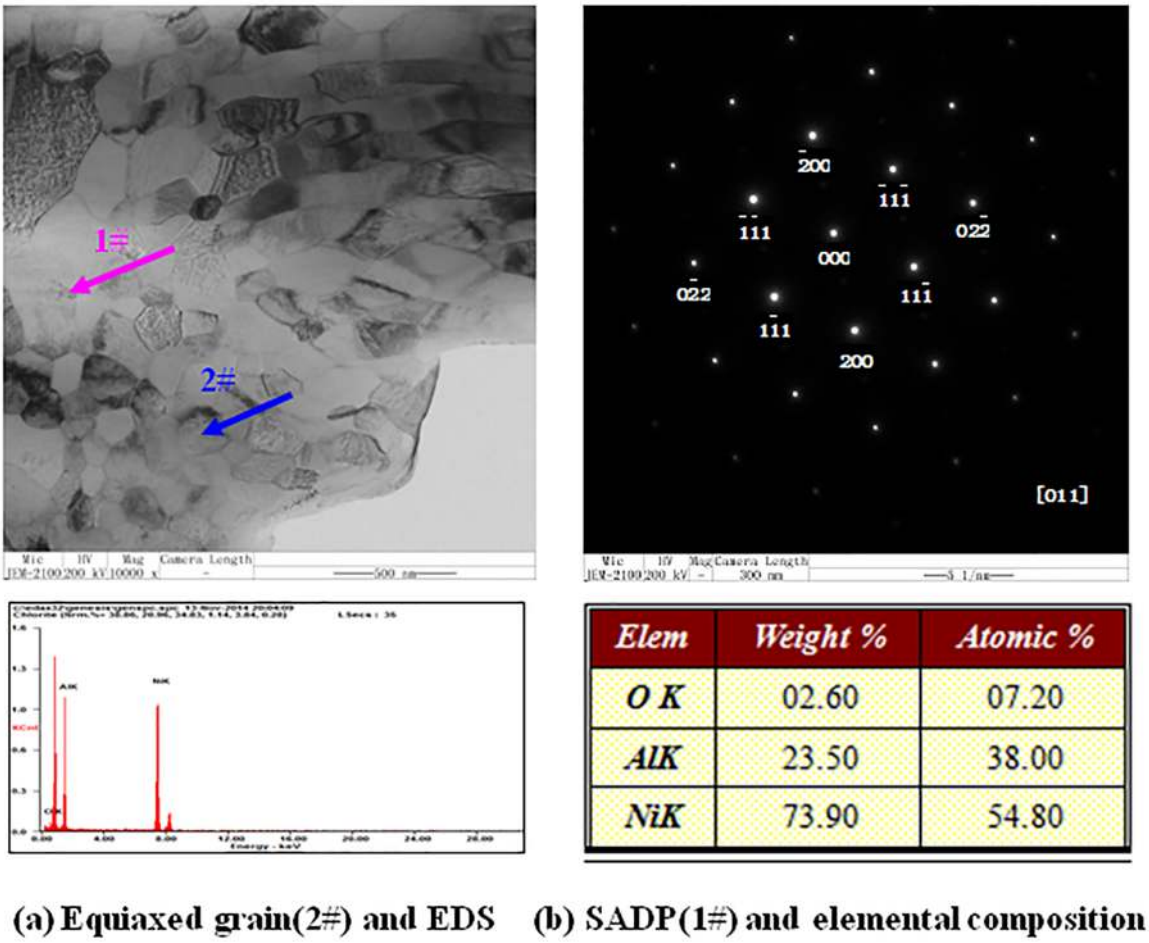

Figure 13. TEM morphology and electron diffraction of the as-prepared coating for (a) and (b).

field emission double-beam scanning electron microscopy was used to further observe the surface morphology of the coating. The process parameters are shown in Table 4. Among them, the bottom layer is Ni-5wt.% Al, the surface layer is Ni-20wt.% Al, the spraying voltage is 30V, and the spraying current is 200A. There are nine different spraying process parameters, the surface layer is expressed by S1~S9.

Figure 14 is the surface morphology and three-dimensional morphology of the coating S2. Figure 14a is the laser confocal microscope to observe the surface morphology, Figure 14b is the SEM morphology, Figure 14c and Figure 14d are the microscope to observe the roughness and three-dimensional morphology of the coating respectively. There are no cracks on the coating surface, and it is uneven and roughness is larger[21, 22].

Table 4. Spraying parameters of Ni-Al coatings.

Layer structure	Air pressure	Gun distance	Gun velocity	Spray frequency	Coating thickness	Surface roughness
	(MPa)	(mm)	(mm/s)		(mm)	(μm)
Ni-5wt.%Al	0.40	150	500	1	0.15~0.25	---
S1	0.40	150	400	2	0.25~0.35	18.042
S2	0.30	150	400	2	0.25~0.35	18.180
S3	0.20	150	400	2	0.25~0.35	24.845
S4	0.40	100	400	2	0.25~0.35	23.558
S5	0.30	100	400	2	0.25~0.35	25.141
S6	0.20	100	400	2	0.25~0.35	31.185
S7	0.40	50	500	1	0.25~0.35	27.282
S8	0.30	50	500	1	0.25~0.35	26.467
S9	0.20	50	500	1	0.25~0.35	27.489

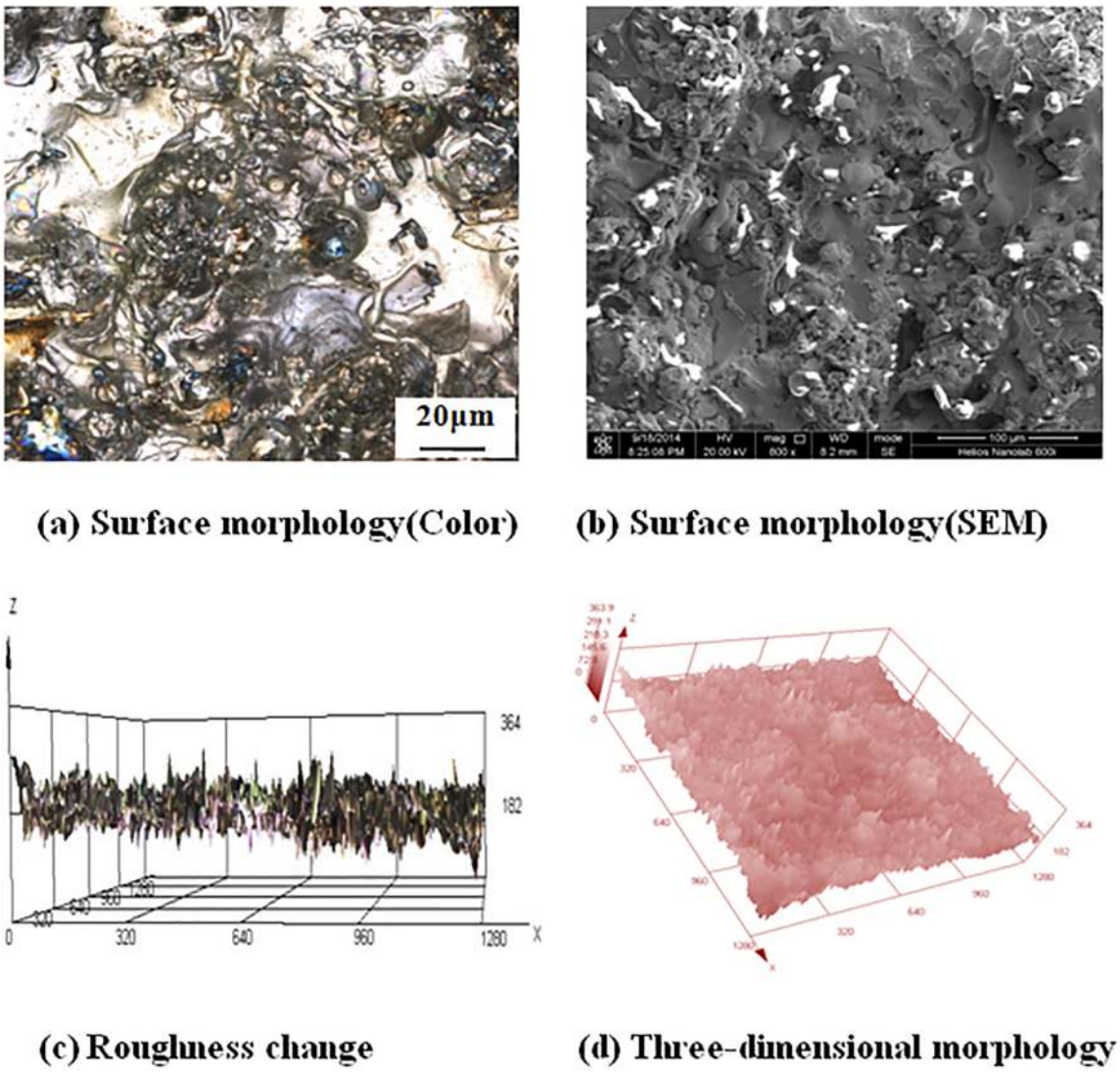

Figure 14. Surface morphology and roughness of Ni-Al coatings for (a), (b), (c) and (d).

It can be seen from Figure 15 and Table 4 that the average surface roughness is 24.688 μm. The surface roughness of S6 coating is the highest, reaching 31.185 μm, the spraying distance of S1 ~ S3 is 150 mm, the spraying distance of S4 ~ S6 is 100 mm, and the spraying distance of S7 ~ S9 is 50 mm. With the decrease of spraying distance, the surface roughness increases. The air pressure of S1 ~ S3 is 0.4 MPa, 0.3 MPa and 0.2 MPa, respectively. The air pressure of S4 ~ S6 and S7 ~ S9 has the same change with S1～S3. With the decrease of air pressure, the surface roughness increases, but with the decrease of spraying distance, the influence of air pressure of spraying decreases.

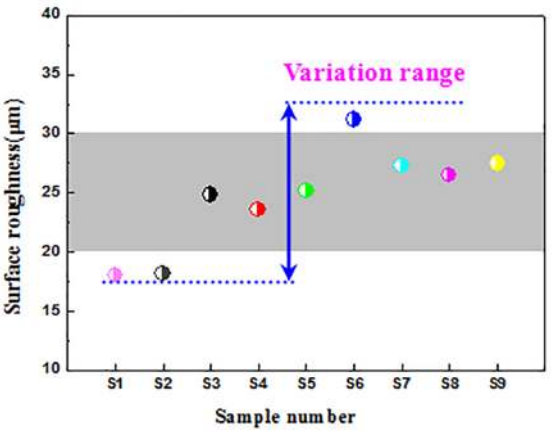

Figure 15. Comparison of surface roughness of Ni-Al coatings for S1-S9.

4. Conclusions

In a certain range, increasing the spraying pressure can increase the droplets flying velocity and improve the droplets

atomization effect. The droplets morphology, solidification layer and temperature field are consistent. The droplets cooling rate ranges from 3.0×10^7 to 7.5×10^7 K/s.

The main components of Ni-5wt.% Al coating are Ni solid solution, and a small number of Ni_3Al_4, Al_2O_3 and NiO. The main phases of Ni-20wt.% Al coating are Ni_3Al and NiAl. The surface roughness increases with the decrease of spraying pressure and spraying distance.

TEM and EDS analysis shows that fine spherical Ni_3Al precipitates are formed in the original substrate Ni solid solution. At the same time, there are amorphous and equiaxed crystals in the original state of the coating, due to the fast cooling process.

5. Acknowledgements

This research work is financially supported by Talent Introduction Project of Guangdong University of Petrochemical Technology (Grant No. 2019rc071) and National Key R&D Program Projects (Grant No. 2016YFB1102102-2). Jixiao Wang would like to thank Prof. Jingtao Sun and Dr. Fujia Xu at the Harbin Welding Institute, China Academy of Machinery Science & Technology, and Prof. Wang Zhiping at the College of science, Civil Aviation University of China, and Dr. Yongxiong Chen, National Engineering Research Center of Mechanical Product Remanufacturing, Academy of Armored Forces Engineering, for their useful suggestions and discussions.

6. References

1. Kelkar M, Heberlein J. Wire-arc spray modeling. *Plasma Chemistry and Plasma Processing.* 2002;22(1):1-25. DOI: https://doi.org/10.1023/A:1012924714157

2. Blackwell BC, Deetjen ME, Gaudio JE, Ewoldt RH. Sticking and splashing in yield-stress fluid drop impacts on coated surfaces. *Physics of Fluids.* 2015;27(4):121-146. DOI: https://doi.org/10.1063/1.4916620

3. Liu J, Xu X. Direct numerical simulation of secondary breakup of liquid drops. *Chinese Journal of Aeronautics.* 2010;23(2):153-161. DOI: https://doi.org/10.1016/S1000-9361(09)60199-0

4. Wang JX, Wang YD, Liu, JS, Zhang, LY, Gao LM, Zheng GH, Shen HX, Sun JF. Microstructure and flight behaviors of droplet and its solidification in twin-wire arc sprayed Ni-Al composite coatings. *Materials Research.* 2018;21(6):1-10. DOI: http://dx.doi.org/10.1590/1980-5373-mr-2017-0394

5. Medřický J, Curry N, Pala Z, Vilemova M, Chraska T, Johansson J, et al. Optimization of high porosity thermal barrier coatings generated with a porosity former. *Journal of Thermal Spray Technology*. 2015;24(4):622-628. DOI: https://doi.org/10.1007/s11666-014-0214-y

6. Foroushani MH, Shamanian M, Salehi M, Davar F. Porosity analysis and oxidation behavior of plasma sprayed YSZ and $YSZ/LaPO_4$ abradable thermal barrier coatings. *Ceramics International*. 2016;42(14):15868-15875. DOI: https://doi.org/10.1016/j.ceramint.2016.07.057

7. Zhang NN, Lin DY, Li YL, Zhang Y, Planche MP, Liao HL. In-flight particle characterization and coating formation under low pressure plasma spray condition. *Journal of Iron and Steel Research, International.* 2017;24(3):306-312. DOI: https://doi.org/10.1016/S1006-706X(17)30044-4

8. Wang JX, Wang GX, Liu JS, Zhang LY, Wang W, Li Z, et al. Microstructure of Ni-Al powders and Ni-Al composite coatings prepared by twin-wire arc spraying. *International Journal of Minerals, Metallurgy and Materials*. 2016;23(7):810-818. DOI: https://doi.org/10.1007/s12613-016-1295-z

9. Kelkar M, Heberlein J. Wire-arc spray modeling. *Plasma Chemistry and Plasma Processing*. 2002;22(1):1-25. DOI: https://doi.org/10.1023/A:1012924714157

10. Hsiang LP, Faeth GM. Near limit drop deformation and secondary breakup. *International Journal of Multiphase Flow*. 1992;18(5):635-652. DOI: https://doi.org/10.1016/0301-9322(92)90036-g

11. Choi HY, Son SW, Yong GP, Ha MY. Effect of droplet size on the droplet behavior on the heterogeneous surface. *Journal of Mechanical Science and Technology*. 2017;31(6):2791-2802. DOI: https://doi.org/10.1007/s12206-017-0522-5

12. Li H, Tao SF, Zhou ZH, Sun LD, Hesnawi A, Gong SK. Element diffusion during fabrication of EB-PVD NiAl coating and its 1100°C isothermal oxidation behavior(II). *Surface and Coatings Technology*. 2007;201(15):6589-6592. DOI: https://doi.org/10.1016/j.surfcoat.2006.09.081

13. Mishra SC, Satapathy A, Chaithanya M, Ananthapadmanabhan PV, Sreekumar KP. Wear characteristics of plasma sprayed nickel-aluminum composite coatings. *Journal of Reinforced Plastics and Composites*. 2009;28(23):2931-2940. DOI: https://doi.org/10.1177/0731684408094067

14. Peng D, Shen J, Tang Q, Wu CP, Zhou YB. Effects of aging treatment and heat input on the microstructures and mechanical properties of TIG-welded 6061-T6 alloy joints. *International Journal of Minerals, Metallurgy, and Materials.* 2013;20(3):259-265. DOI: https://doi.org/10.1007/s12613-013-0721-8

15. Tillmann W, Abdulgader M. Particle size distribution of the filling powder in cored wires: its effect on arc behavior, in-flight particle behavior, and splat formation. *Journal of Thermal Spray Technology*. 2012;21(3-4):706-718. DOI: https://doi.org/10.1007/s11666-012-9769-7

16. Gedzevicius I, Valiulis AV. Analysis of wire arc spraying process variables on coatings properties. *Journal of Materials Processing Technology*. 2006;175(1-3):206-211. DOI: https://doi.org/10.1016/j.jmatprotec.2005.04.019

17. Zhang LM, Liu BW, Sun DB. Preparation and properties of the Ni-Al/Fe-Al intermetallics composite coating produced by plasma cladding. *International Journal of Minerals, Metallurgy, and Materials*. 2011;18(6):725-730. DOI: https://doi.org/10.1007/s12613-011-0503-0

18. Feng RB, Gong SJ, Peng J. Contrastive study of wear and friction on Ni-5wt%Al and Ni-20wt%Al coating. *Rare Metal Materials and Engineering*. 2011;40(Suppl 3):269-272. DOI: https://doi.org/10.1002/maco.201005741

19. Luo L, Liu S, Li J, Wu Y. Thermal shock resistance of $FeMnCrAl/Cr_3C_2$–Ni9Al coatings deposited by high velocity arc spraying. *Surface and Coatings Technology*. 2011;205(11):3467-3471. DOI: https://doi.org/10.1016/j.surfcoat.2010.12.014

20. Vencl A, Arostegui S, Favaro G, Zivic F, Mrdak M, Mitrovi S, et al. Evaluation of adhesion/cohesion bond strength of the thick plasma spray coatings by scratch testing on coatings cross-sections. *Tribology International*. 2011;44(11):1281-1288. DOI: https://doi.org/10.1016/j.triboint.2011.04.002

21. Celik C, Cehreli BS, Bagis B, Arhun N. Microtensile bond strength of composite-to-composite repair with different surface treatments and adhesive systems. *Journal of Adhesion Science and Technology*. 2014;28(13):1264-1276. DOI: https://doi.org/10.1080/01694243.2014.896069

22. Wang JX, Liu JS, Zhang LY, Sun JF, Wang ZP. Microstructure and mechanical properties of twin-wire arc sprayed Ni-Al composite coatings on 6061-T6 aluminum sheet. *International Journal of Minerals, Metallurgy and Materials*. 2014;21(5):469-478. DOI: https://doi.org/10.1007/s12613-014-0931-8